SMOS ocean salinity: recent improvements and applications

Xiaobin Yin[1,2], Jacqueline Boutin[1], Jordi Font[3], Nicolas Reul[4], Paul Spurgeon[2], Jean-Luc Vergely[5] and Nicolas Martin[1]*

[1]LOCEAN, UPMC- Tour 45-55-5eme etage, 4, place Jussieu, 75252 Paris, France. xylod@locean-ipsl.upmc.fr, jb@locean-ipsl.upmc.fr and martin@locean-ipsl.upmc.fr
[2]ARGANS, 1 Davy Road, Tamar Science Park, PL6 8BX Plymouth, UK. PSpurgeon@argans.co.uk
[3]ICM-CSIC, Passeig Maritim 37-49, 08003 Barcelona, Spain. jfont@icm.csic.es
[4]IFREMER, Zone Portuaire de Brégaillon, 83507 La Seyne-sur-Mer, France. Nicolas.Reul@ifremer.fr
[5]ACRI-ST, 260 route du Pin Montard, Sophia Antipolis, France. jeanluc.vergely@aerov.jussieu.fr

Abstract

The European Space Agency's Soil Moisture and Ocean Salinity (SMOS) mission, launched in November 2009, has been providing global maps of sea surface salinity (SSS) since 2010. The SMOS SSS derived with version 5 reprocessing senses realistic SSS variability at various time and space scales, although some biases remain a basin and seasonal scale. In this paper, after providing an overview of the SMOS version 5 SSS quality derived from comparisons with in situ measurements, we provide examples of the observed variability associated with tropical instability waves during 2010 and 2013. Then we show improvements expected in future SMOS level 2 reprocessing coming from a new method for retrieving Total Electron Content (TEC). We also estimate the SMOS SSS uncertainties due to uncertainties in *a priori* sea surface temperature (SST) and wind speed (WS), especially in the tropical Pacific Ocean where there are significant and sometimes coupled variations of SST and WS due to strong seasonal upwelling, zonal surface currents and the development of tropical instability waves.

1. Introduction

The ocean is the dominant element of the global water cycle because 78% of the precipitation and 86% of the evaporation over the globe take place above the ocean and the river discharges flow from the land to the ocean [1]. In addition, salinity and temperature determine the density of sea water so that salinity is a key parameter for studying the formation and circulation of water masses. Until recently it was only possible to measure the salinity in-situ. The recent development of sea surface salinity (SSS) observations with satellite L-band radiometers is one of the most promising tools to improve climate modeling and prediction. Two L-band satellite missions aimed at observing SSS from space have been launched in November 2009 (the European Soil Moisture and Ocean Salinity (SMOS) mission [2]) and in June 2011 (the Aquarius mission [3]). The SSS can be measured in-situ over a practical salinity scale (pss hereafter), which corresponds to the conductivity ratio of a sea water sample to a standard potassium chloride solution [4].

In this paper, introduction of retrievals with SMOS is presented in section 2, the quality of SMOS version 5 SSS is presented in section 3, SMOS SSS signatures of tropical instability waves are presented in section 4, improvements expected in future SMOS level 2 reprocessing coming from a new method for retrieving Total Electron Content (TEC) are presented in section 5, the SMOS SSS uncertainties due to uncertainties in *a priori* sea surface temperature (SST) and wind speed (WS) are estimated in section 6, and results are summarized in section 7.

2. Retrievals with SMOS

The SMOS 2-D interferometric concept [2] allows the instrument to perform measurements over 2-D snapshots so that a grid point over the ocean is seen by numerous independent snapshots under various incidence and azimuth angles. The retrievals are based on the Levenberg and Marquardt iterative convergence method. The first guess geophysical inputs (SSS, SST, WS and TEC) are adjusted in order to minimize a "cost function" χ^2 expressed by

$$\chi^2 = \sum_{i=1}^{N} \frac{\left[TB_i^{meas} - TB_i^{mod}\right]^2}{\sigma_{TB_i}^2} + \sum_{j=1}^{Np} \frac{\left[P_j - P_j^{prior}\right]^2}{\sigma_{P_j}^2}, \quad (2)$$

where N is the number of TBs (TB_i^{meas}) available for the SSS retrieval at different incidence angles θ_i for the four Stokes parameters (TX, TY, T3 and T4) in the antenna frame as detailed in [5], TB_i^{mod} is the TB simulated at incidence angles θ_i, and $\sigma_{TB_i}^2$ is the expected variance of the differences between TB_i^{meas} and TB_i^{mod} given the instrumental radiometric resolution of TBs and estimates of the model error. P_j are the retrieved parameters, in the case studied: SSS, SST, WS and TEC. P_j^{prior} is an *a priori* estimate of the P_j with an *a priori* variance $\sigma_{P_j}^2$.

The forward model implemented in the ESA L2OS processor simulates the flat sea emission with the Klein and Swift (1977) model [6] and other contributions from the rough sea surface [7, 8 and J. Tenerelli personal comm.], the atmospheric emission and absorption [9], and the scattering of galactic noise [J. Tenerelli personal comm.] and of atmospheric radiation by the ocean surface.

978-1-4673-5225-3/14/$31.00 ©2014 IEEE

3. Quality of SMOS Version 5 SSS

SMOS SSS are collocated with in situ SSS of the Array for Real-Time Geostrophic Oceanography (ARGO) floats within a radius of 50km and 5 days, following the same flag sorting as the one described in [10] and after excluding SMOS SSS at less than 700km from the coast where large biases in SMOS SSS are observed. The spatial distribution of ARGO floats is shown in Fig. 1 and Table 1 presents statistics of the differences obtained for May 2011. On ascending orbits, in subtropical and tropical regions (see an example line 3 in Table 1) the standard deviation (std) of the difference is about 0.2 but it degrades when including colder waters. Std is systematically worse over descending orbits than over ascending ones. Latitudinal biases also appear on the global maps (Fig. 1).

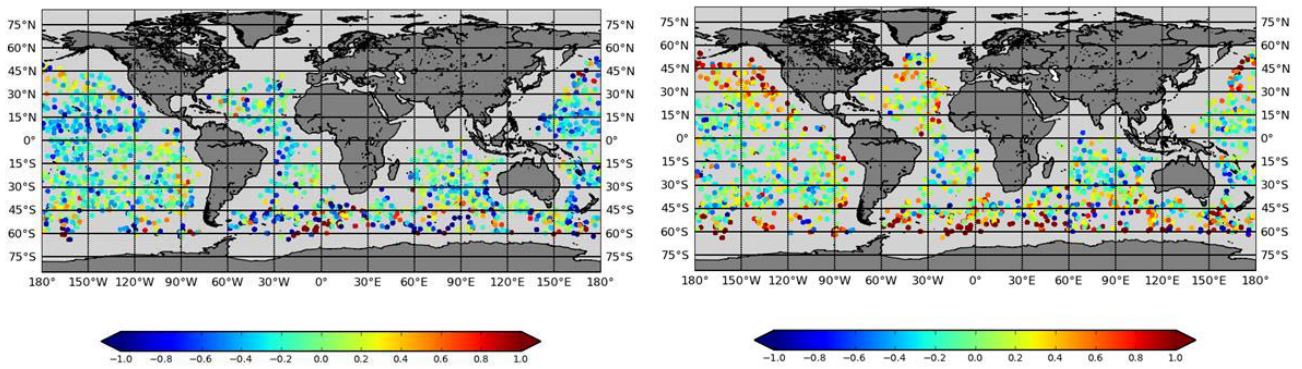

Fig. 1 SMOS minus ARGO SSS rms error using SMOS ascending orbits (left) and descending orbits (right) in May 2011.

Table 1 Statistics of SMOS-ARGO SSS differences - SMOS L2 v550 - May 2011

		Ascending orbits			Descending orbits		
Region	Zone	N	Mean (pss)	std(pss)	N	Mean (pss)	std(pss)
Global	60S60N-180W180E	2387	-0.11	0.44	2207	0.14	0.51
45°S-45°N	45S45N-180W180E	1932	-0.13	0.34	1687	0.07	0.42
Tropical	30S30N-180W180E	1270	-0.17	0.31	1042	0.00	0.34
Southern Pacific	30S0N-150W120W	101	-0.09	0.22	68	-0.04	0.26

4. SMOS Sea Surface Salinity signatures of tropical instability waves

Cusp-shaped wave patterns associated with tropical instability waves (TIWs) are clearly seen both in the SMOS SSS and the Operational Sea Surface Temperature and Sea Ice Analysis (OSTIA) SST (white boxes in Fig. 2), though the SSS cusps are not as sharp as the SST cusps given smoothing of the SSS data. The SSS cusps are noticeable in the northern hemisphere, with the northward higher SSS cusps coinciding with that of lower SST.

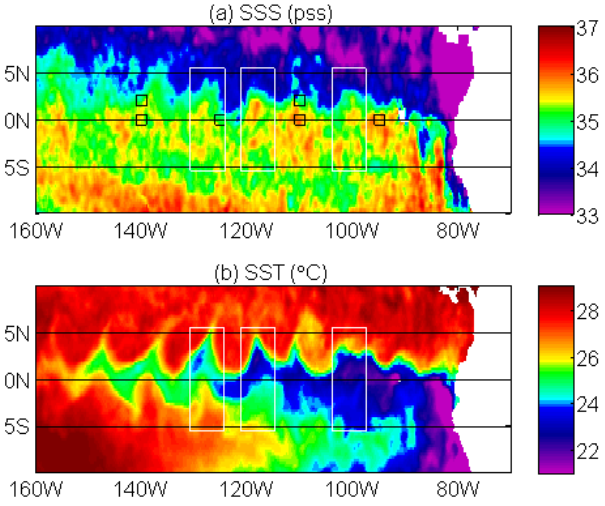

Fig. 2 10-day average SMOS SSS centered on June 26, 2010 (a) and daily OSTIA SST on the same date (b). The white boxed indicate regions where cusp-shaped wave patterns are clearly seen.

SSS measurements from the SMOS satellite from June 2010 to May 2013 provide an unprecedented space-borne observation of the salinity structure of TIWs during strong, moderate and non- La Niña years. The related SSS signature has approximate peak amplitude of 0.5 pss. Westward propagations of SMOS SSS signatures appeared west of 90°W seasonally and the intensity of the waves is much stronger when the indices in the NINO1+2, NINO3 and NINO3.4 regions are negative than the period when the indices are positive. The amplitudes and extents of SSS signatures decreased year by year from 2010 to 2013. The westward propagation speed of SSS is approximately between 0.6 m/s and 1.5 m/s depending on latitude and dominant period of TIWs.

5. TEC estimate in future reprocessing

A main source of uncertainty for retrieving SSS on descending orbits comes from the correction of the Faraday rotation. A new method for deriving TEC from SMOS Stokes 3 measurements has been implemented in the new version 6 of the level 2 SMOS ocean salinity (L2OS) processor. A substantial improvement has been obtained in the derivation of the so-called ocean target transformation [5] used for correcting systematic biases of SMOS brightness temperatures. With this method implemented, the SMOS SSS retrieved on descending orbits become of better quality and closer to the quality of SMOS SSS retrieved on ascending orbits (Table 1 and Table 2).

Table 2 Statistics of SMOS-ARGO differences – SMOS descending orbits – SMOS L2 v611 - May 2011

		Descending orbits		
Region	Zone	N	Mean (pss)	std(pss)
Global	60S60N-180W180E	1977	-0.02	0.50
45°S-45°N	45S45N-180W180E	1527	-0.03	0.38
Tropical	30S30N-180W180E	952	-0.05	0.30
Southern Pacific	30S0N-150W120W	61	0.00	0.20

6. SMOS SSS uncertainties associated with errors on auxiliary parameters

One main geophysical source of error in the retrieval of SSS from L-band TB comes from the need for correcting the effect of the surface roughness and foam. In the SMOS processing, WS provided by the European Centre for Medium-Range Weather Forecasts (ECMWF) is used to initialize the retrieval process of WS and SSS. This process compensates for the lack of onboard instrument providing a measure of ocean surface WS independent of the L-band radiometer measurements. Using multi-angular polarimetric SMOS TBs, it is possible to adjust the WS from the initial value in the center of the swath (within ±300km) by taking advantage of the different sensitivities of L-band H-pol and V-pol TBs to WS and SSS at various incidence angles. As a consequence, the inconsistencies between the MIRAS sensed roughness and the roughness simulated with the ECMWF WS are reduced by the retrieval scheme but they still lead to residual biases in the SMOS SSS [11]. We have developed an alternative two-step method for retrieving WS from SMOS TB, with larger error on prior ECMWF wind speed in a first step. It improves SSS in some areas characterized by large currents, although it is more sensitive to SMOS TB errors in the vicinity of coasts.

The SST used in the SMOS SSS retrievals is from ECMWF Meteorological Archival and Retrieval System (MARS) archive which uses the OSTIA SST. There are noticeable differences between the OSTIA SST and the Reynolds SST [12], which can lead to noticeable differences in retrieved SSS especially in cold water (Fig .3).

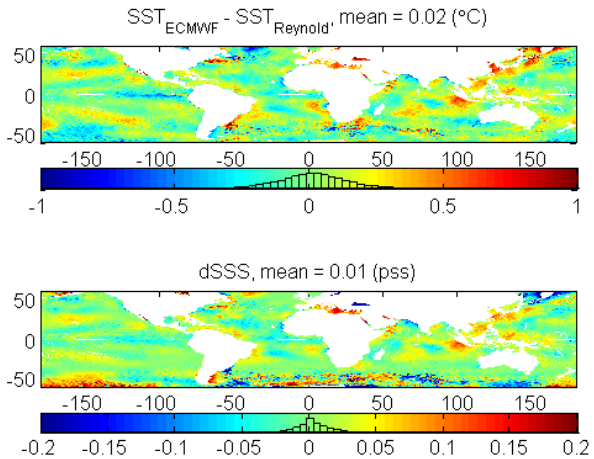

Fig. 3 Differences between monthly ECMWF SST and Reynolds SST maps (top), and the corresponding estimated SSS error (bottom) in August 2010.

7. Conclusion

While seasonal and latitudinal biases remain in SMOS version 5 SSS, the SSS variability at a few hundreds of km is very well caught by SMOS and improves our knowledge of SSS variability such as tropical instability waves. Westward propagations of SMOS SSS signatures appeared west of 90°W seasonally and the amplitudes and extents of SSS signatures decreased year by year from 2010 to 2013. A new method for retrieving TEC is implemented in L2OS v6 and is expected to significantly improve SMOS retrieved SSS on descending orbits. A two-step method for retrieving WS from SMOS TB improves SSS in some areas characterized by large currents. Differences between the OSTIA SST and Reynolds SST product can lead to noticeable differences in retrieved SSS especially in cold water. Further study of the impact of uncertainties in *a priori* SST and WS on SMOS SSS uncertainties is needed.

8. Acknowledgments

This work was funded by the European Space Agency (ESA) Support to Science element project entitled SMOS+Surface Ocean and Synergy, by the CNES/TOSCA/SMOS-GLOSCAL project and by the European Space Agency expert support laboratory project. The ARGO data are provided by CORIOLIS.

9. References

1. R. Schmitt, “Salinity and the global water cycle,” *Oceanography*, **21(1)**, 2008, pp. 12–19.
2. Y. Kerr, P. Waldteufel, et al., “The SMOS mission: A new tool for monitoring key elements of the global water cycle,” *Proceedings of the IEEE*, **98(5)**, 2010, pp. 666–687.
3. D. Le Vine, G. Lagerloef and S. Torrusio, “Aquarius and remote sensing of sea surface salinity from space,” Proceedings of the IEEE, **98(5)**, 2010, 688–703.
4. Unesco, “Background papers and supporting data on the Practical Salinity Scale 1978”, Technical Papers in Marine Science, **37**, 1981, pp. 144.
5. X. Yin, J. Boutin, and P. Spurgeon, “First assessment of SMOS data over open ocean: Part I—Pacific ocean,” IEEE Trans. Geosci. Remote Sens., **50(5)**, May 2012, pp. 1648–1661.
6. L. Klein and C. Swift, “An improved model for the dielectric constant of sea water at microwave frequencies,” *IEEE Trans. Antennas and Propagation*, **AP-25(1)**, 1977, pp. 104–111.
7. X. Yin, J. Boutin, et al., “Optimization of L-band sea surface emissivity models deduced from SMOS data,” *IEEE Trans. Geoscience and Remote Sensing*, **50(5)**, May 2012, pp. 1414–1426.
8. S. Guimbard, J.Gourrion, et al., “SMOS semi-empirical ocean forward model adjustment,” *IEEE Trans. Geoscience and Remote Sensing*, **50(5)**, May 2012, pp. 1676-1687.
9. H. Liebe, G. Hufford and M. Cotton, “Propagation modeling of moist air and suspended water/ice particles at frequencies below 1000 GHz,” Proc. NATO/AGARD Wave Propagation Panel, 52nd meeting, **3**, 1993, pp. 1-10.
10. J. Boutin, N. Martin, G. Reverdin, X. Yin and F. Gaillard, “Sea surface freshening inferred from SMOS and ARGO salinity: Impact of rain,” *Ocean Sci.*, **9**, 2013, pp. 183-192.
11. X. Yin, J. Boutin, et al., “Errors in SMOS Sea Surface Salinity and their dependency on a priori wind speed,” *Remote Sensing of Environment*, doi: j.rse.2013.09.008, in press
12. R. Reynolds, T. Smith, et al., “Daily high-resolution-blended analyses for sea surface temperature,” *J. Clim.*, **20**, 2007, pp. 5473–5496.